ELSEVIER

Contents lists available at ScienceDirect

International Journal of Non-Linear Mechanics

journal homepage: www.elsevier.com/locate/nlm





A finite strain integral model for the creep behavior of vaginal tissue

Justin Dubik ^a, Alfonsina Tartaglione ^b, Alan Wineman ^c, David Dillard ^a, Raffaella De Vita ^{a,*}

- ^a Department of Biomedical Engineering and Mechanics, 325 Stanger Street, Blacksburg, 24061, VA, United States
- b Department of Mathematics and Physics, Università degli Studi della Campania Luigi Vanvitelli, Viale Abramo Lincoln 5, Caserta, 81100, Italy
- ^c Department of Mechanical Engineering, University of Michigan, 2350 Hayward, Ann Arbor, 48109, MI, USA

ARTICLE INFO

Keywords:
Constitutive model
Finite strain
Integral theory
Biaxial creep
Inflation
Vaginal tissue

ABSTRACT

Vaginal delivery causes significant stretching of the vagina and surrounding muscles, potentially leading to the development of pelvic floor disorders and other maternal morbidities. Despite the extended duration of labor, little experimental and theoretical work has been done to characterize the long-term viscoelastic behavior of vaginal tissue. To mathematically capture the creep response of rat vaginal tissue measured, this study presents a new anisotropic finite-strain constitutive model within the single integral Pipkin-Rogers viscoelastic framework. The constitutive parameters are computed by curve-fitting the model to strain versus time data collected from *ex vivo* inflation testing along the two primary anatomical directions of the vagina, the longitudinal and circumferential directions. The results showed good agreement between theory and experiments, suggesting that the proposed model could be used to advance our understanding of the time-dependent deformations that are experienced by the vagina during delivery. This modeling framework represents a first step toward the development of accurate computational tools that can predict the safety of vaginal deliveries, reducing unnecessary Cesarean sections and their related complications.

1. Introduction

Vaginal delivery is a natural physiological process that induces extreme changes in the vagina, potentially leading to many health complications later in a woman's life. Of the nearly 2.5 million women who undergo vaginal delivery annually in the United States [1], a notable 30% will experience at least one pelvic floor disorder later in life. This incidence is notably higher when contrasted with the 11% occurrence observed in women who have never been pregnant [2]. The fear of childbirth has led to an increasing number of elective Cesarean procedures in the United States [3,4]. This in turn has contributed to the country having one of the highest Cesarean rates in the world [1,5], resulting in a substantial increase in the average cost of childbirth [6]. The Cesarean delivery is an alternative procedure to vaginal delivery which is associated with its own set of risks and potential complications such as uterine rupture and the need for a hysterectomy [7]. Opting for a C-section does not conclusively eliminate the risk of the same health issues that some women seek to avoid through elective C-sections [8,9].

Detailed knowledge of the properties of the pelvic floor organs and tissues is necessary for gaining insight into the mechanics of child-birth and for the development of effective tools to improve maternal care. Vaginal delivery is a biomechanically intensive event that places the pelvic floor organs and surrounding tissues under prolonged and significant stress and stretching [10]. The vagina in particular can

significantly stretch over time, going from a reference diameter of roughly 2.5 cm up to a diameter of nearly 10 cm within the second stage of labor [11]. While studies of the biomechanical behavior of vaginal tissue have been performed [12], insufficient attention has been given to characterizing the viscoelastic properties of this tissue, which undoubtedly play a crucial role during extended biomechanical processes like childbirth. In particular, the development of constitutive models that can describe the creep response (i.e., the time-dependent increase in deformation under constant load) of the vagina is crucial for the advancement of computational tools aimed at modeling and comprehending the complexities of vaginal delivery.

The characteristic mechanical behavior of the vagina is primarily attributed to its complex and heterogeneous microstructure [13,14]. In both humans and other mammals [15], the primary components of this organ, including collagen, smooth muscle, and elastin fibers, play a crucial role in determining the biomechanical properties of the organ, including the viscoelastic behavior. Previous experimental studies, performed on cadaveric tissue and other animal tissue, have revealed several viscoelastic phenomena in vaginal tissue. In a preliminary study that established a consistent protocol for uniaxial tensile testing, Rubod et al. observed that the rate of deformation can have a significant influence on the mechanical response of ewe vaginal tissue [16]. Multiple other studies have utilized uniaxial tensile testing to observe

^{*} Corresponding author.

E-mail address: devita@vt.edu (R. De Vita).

Mullins-type softening of vaginal tissue from both humans and other animal species, a phenomenon resulting from cyclic loading [17–20]. Uniaxial testing has also been employed to quantify stress relaxation (i.e., decrease in stress over time at constant deformation) of the human vaginal tissue [21].

Over the past few years, alternative experimental methods for testing the mechanical properties of the vagina have gained popularity due to their ability to replicate more physiologically relevant loading conditions. Pack et al. utilized planar biaxial testing to measure the stress relaxation behavior of gilt vaginal tissue simultaneously stretched along the two primary anatomical directions of the vagina, the longitudinal direction (LD) and circumferential direction (CD) [22]. Retaining the vagina's original anatomical geometry of a cylinder, Clark-Patterson et al. performed biaxial inflation testing at variable fixed axial deformations, investigating how strain coupling between the LD and CD may affect creep behavior of mice vaginal tissue [23]. Clark-Patterson et al. also recently investigated the creep behavior of mice vaginal canals in their active state (i.e., while the organ is contracted) using a similar setup, observing that more creep strain occurred in the active state than in the passive tissue [24]. Finally, our lab has conducted free-extension inflation tests to quantify the creep behavior of the rat vagina in both the LD and CD in response to consecutive and increasing loading pressures. In particular, we observed key differences in the elastic and viscoelastic behavior between the two loading directions, and that both the short-term and long-term creep behaviors of the vaginal tissue depended on the loading history [25].

The isotropic elastic properties of the vagina have been modeled using the Mooney-Rivlin constitutive equation [20,26-28]. While the use of this model helped the comparisons of elastic parameters between groups (e.g., prolapsed versus non-prolapsed tissue), constitutive equations that capture the anisotropic and viscoelastic behavior of vaginal tissue are more accurate. Martins et al. successfully used a transversely isotropic model to describe the response of prolapsed human vaginal tissue under tension in the LD [29]. Akintunde et al. demonstrated that the Holzapfel-Gasser-Ogden model with two fiber families can be applied to model the mechanical response of murine vaginal tissue to inflation [30]. Calvo et al. [31] and Peña et al. [18] proposed new anisotropic models that incorporate the description of damage to reproduce the experimentally observed mechanical response of prolapsed human vaginal tissue to uniaxial cyclic loading in the LD and CD [18,31]. Finally, Peña et al. presented an anisotropic viscoelastic model for the stress relaxation behavior of prolapsed human vaginal tissue elongated along the LD [21]. To our knowledge, despite some progress being made on collecting creep data [23-25], there are no constitutive models that reproduce the experimentally measured biaxial creep response of vaginal tissue by accounting for the tissue's anisotropy, nonlinearity, and large deformations.

One of the most common approaches used in modeling the viscoelasticity of soft biological tissue is the rheological approach, where the creep behavior is modeled as a combination of springs and dashpots [32–34]. More popular for high fidelity modeling, however, are mathematical formulations in continuum mechanics, particularly for modeling large deformations in three-dimensions. The viscoelastic continuum models can generally be described by three categories: differential-type, rate-type, and integral-type equations [35]. Differentialtype equations, in which the stress of a material depends only on recent deformations and deformation rates, have been utilized before [36, 371, but are insufficient in cases where the mechanical behavior is history-dependent [35]. Rate-type viscoelastic models, in which the current stress depends on both recent deformations and recent stress history, are quite popular due to their relatively low computational complexity [38]. Finally, integral formulations describe the stress or deformation behavior of materials in the form of integrals in order to account for the complete stretch or stress history. While computationally expensive, their accuracy in capturing the response of materials whose mechanical behavior varies with loading/deformation history is

valuable. Because of this, such models have been proposed to describe the three-dimensional creep behavior of non-biological soft bodies [39], and such integral formulations have been used for describing the creep and relaxation behavior of ligaments [40–42]. However, the full three-dimensional formulations have gone largely unused for describing creep behavior of soft tissues [43].

In this study, we present a three-dimensional constitutive model that describes the creep behavior of vaginal tissue within the integral formulation established by Pipkin and Rogers [44]. We selected the integral formulation since we have observed that the creep response of vaginal tissue depends on the loading history by conducting inflation tests at three progressively increasing pressures on rat vaginas [25]. In this formulation, the vaginal tissue undergoes large deformations while being in a state of plane stress that results from the thin-walled pressure vessel assumptions. The creep behavior of the vaginal tissue is modeled by the use of a separable nonlinear viscoelastic anisotropic model with axes of material symmetry which coincide with the organ's natural anatomical directions, the LD and CD. We evaluate the constitutive model using experimentally collected strain versus time data along LD and CD. This modeling framework represents a significant step toward the development of accurate constitutive models which could lead to computational tools that guide decisions about the optimal delivery method for expectant women.

2. Modeling framework

In this section, we provide a brief overview of the nonlinear integral representation theory for viscoelastic materials that is presented in great detail by Pipkin and Rogers [44]. Specifically, we first represent the creep response in terms of the stress history (Section 2.1). Then, we provide a general form of the creep kernel function by accounting for the material properties of vaginal tissue and the organization of the fibers in the two main physiological loading directions of the vagina: the LD and the CD (Section 2.2).

2.1. Creep

The most general constitutive equation for a non-aging viscoelastic material takes the following form [45]:

$$\sigma(t) = \mathcal{F}[\mathbf{F}(t-\tau)|_{\tau=0}^{\infty}], \tag{1}$$

where σ is the Cauchy stress tensor, F is the deformation gradient, and F is a tensor-valued response functional representing the dependence of the stress on the deformation history up to time t. By applying the invariance under superposed rigid body motions, Eq. (1) can be rewritten as [43]

$$\mathbf{S}(t) = \mathcal{F}[\mathbf{C}(t-\tau)|_{\tau=0}^{\infty}], \tag{2}$$

where $\mathbf{S} = J\mathbf{F}^{-1}\sigma\mathbf{F}^{-T}$, with $J = \det(\mathbf{F})$, is the second Piola–Kirchhoff stress tensor and $\mathbf{C} = \mathbf{F}^T\mathbf{F}$ is the right Cauchy–Green deformation tensor, with an obviously new meaning for \mathcal{F} .

The constitutive Eq. (2) can be used to describe the results of stress relaxation experiments. In order to describe the results of creep tests, the following constitutive equation can be used:

$$\mathbf{C}(t) = \mathcal{G}[\mathbf{S}(t-\tau)|_{\tau=0}^{\infty}], \tag{3}$$

where \mathcal{G} is a tensor-valued response functional that describes the dependence of the strain on the stress history up to time t. Eq. (3), which is the dual counterpart of Eq. (2), represents the deformation resulting from a given stress history while also satisfying the principle of material frame-indifference. To show this, let $\overline{\mathbf{F}}$ and $\overline{\sigma}$ be linked to \mathbf{F} and σ , respectively, by a rotation tensor \mathbf{Q} (i.e., $\overline{\mathbf{F}} = \mathbf{Q}\mathbf{F}$ and $\overline{\sigma} = \mathbf{Q}\sigma\mathbf{Q}^T$). Noting that $\overline{J} = \det(\overline{\mathbf{F}}) = \det(\mathbf{F}) = J$, then

$$\mathcal{G}[\overline{\mathbf{S}}(t-\tau)|_{\tau=0}^{\infty}] = \mathcal{G}[\overline{J}\overline{\mathbf{F}}^{-1}\overline{\sigma}\overline{\mathbf{F}}^{-T}(t-\tau)|_{\tau=0}^{\infty}]
= \mathcal{G}[\overline{J}\overline{\mathbf{F}}^{-1}\mathbf{Q}^{-1}\mathbf{Q}\sigma\mathbf{Q}^{T}\mathbf{Q}^{-T}\mathbf{F}^{-T}(t-\tau)|_{\tau=0}^{\infty}] =
\mathcal{G}[J\mathbf{F}^{-1}\sigma\mathbf{F}^{-T}(t-\tau)|_{\tau=0}^{\infty}] = \mathcal{G}[\mathbf{S}(t-\tau)|_{\tau=0}^{\infty}] = \mathbf{C}(t) = \overline{\mathbf{C}}(t).$$
(4)

It is worth noting here that G may be expressed as a function of both S and the invariants of S [46].

Based on previous research on modeling the viscoelasticity of soft tissues [43,47], we select the most general constitutive model to describe the creep behavior of vaginal tissue, that is the Pipkin and Rogers integral representation [44]. According to this representation, Eq. (3) can be expressed as the following integral series:

$$\mathbf{C}(t) = \sum_{n=1}^{\infty} \mathbf{E}_n(t) , \qquad (5)$$

where E, is defined as follows:

$$\mathbf{E}_{n}(t) = \frac{1}{n!} \int_{-\infty}^{t} ... \int_{-\infty}^{t} d\mathbf{S}(\tau_{1}) ... d\mathbf{S}(\tau_{n}) \mathbf{K}_{n}[\mathbf{S}(\tau_{1}), t - \tau_{1}; ...; \mathbf{S}(\tau_{n}), t - \tau_{n}].$$
 (6)

In Eq. (6), K_n is the nth creep kernel and $d_{\mathbf{S}(\tau_i)}$ $(i=1,\ldots,n)$ denotes the operator defined as

$$d_{\mathbf{S}(\tau_i)}f[\mathbf{S}(\tau_1), t - \tau_1; ...; \mathbf{S}(\tau_n), t - \tau_n] = \frac{\partial f}{\partial \mathbf{S}(\tau_i)}\mathbf{S}'(\tau_i)d\tau_i \tag{7}$$

at times τ_i for which S is differentiable. \mathbf{K}_1 represents the single-step creep function, which is the deformation arising from a single-step stress history, in which the stress is instantaneously changed from zero and then held constant. For $n \geq 2$, \mathbf{K}_n is the correction function resulting from error in predicting the strain for an n-step history from (n-1)-step data. Further discussion about the properties of this error are presented in the seminal paper by Pipkin and Rogers [44].

We approximate Eq. (5) with only the first term \mathbf{E}_1 of the integral series so that $\mathbf{C}(t) = \mathbf{E}_1(t)$. Since the subscript 1 is now superfluous, we have that the strain can be represented by

$$\mathbf{C}(t) = \int_{-\infty}^{t} d_{\mathbf{S}(\tau)} \mathbf{K}[\mathbf{S}(\tau), t - \tau], \qquad (8)$$

or, equivalently,

$$\mathbf{C}(t) = \int_{-\infty}^{t} \frac{\partial \mathbf{K}}{\partial \mathbf{S}(\tau)} [\mathbf{S}(\tau), t - \tau] \mathbf{S}'(\tau) d\tau . \tag{9}$$

The single-integral representation provided in Eq. (9) is the extension as $n \to +\infty$ corresponding to an arbitrary stress history $\mathbf{S}(\tau)$ resulting from step increases in stress that is defined by $\mathbf{S}_1, \mathbf{S}_2, ..., \mathbf{S}_n$, with each \mathbf{S}_i constant in the interval $[t_i, t_{i+1})$ when strain is represented only by using the single step creep function $\mathbf{K}_1[\mathbf{S}, t] = \mathbf{K}[\mathbf{S}, t]$, leading to the extrapolation rule:

$$\mathbf{E}_{1}(t) = \sum_{i=1}^{n} \mathbf{K}[\mathbf{S}_{i}, t - t_{i}] - \mathbf{K}[\mathbf{S}_{i-1}, t - t_{i}].$$
 (10)

As noted by Pipkin and Rogers [44], Eq. (10) corresponds to a modified superposition rule.

We assume that K[0, s] = 1, where 1 is the identity tensor, for all s and that S(s) = 0 for all s < 0. Moreover, we assume that a jump discontinuity at t = 0 for the stress history may occur and we denote

$$S(0) = S(0^+) - S(0^-) = S(0^+)$$
.

Starting from Eq. (9), one has

$$\mathbf{C}(t) = \int_{-\infty}^{0} \frac{\partial \mathbf{K}}{\partial \mathbf{S}(\tau)} [\mathbf{S}(\tau), t - \tau] \mathbf{S}'(\tau) d\tau + \mathbf{K} [\mathbf{S}(0^{+}), t] - \mathbf{K} [\mathbf{S}(0^{-}), t]$$

$$+ \int_{0}^{t} \frac{\partial \mathbf{K}}{\partial \mathbf{S}(\tau)} [\mathbf{S}(\tau), t - \tau] \mathbf{S}'(\tau) d\tau = \mathbf{K} [\mathbf{S}(0), t] + \int_{0}^{t} \frac{\partial \mathbf{K}}{\partial \mathbf{S}(\tau)} [\mathbf{S}(\tau), t - \tau] \mathbf{S}'(\tau) d\tau .$$

$$(11)$$

From the following total derivative:

$$\frac{d}{d\tau}\mathbf{K}[\mathbf{S}(\tau), t - \tau] = \frac{\partial \mathbf{K}}{\partial \mathbf{S}(\tau)}[\mathbf{S}(\tau), t - \tau]\mathbf{S}'(\tau) - \frac{\partial \mathbf{K}}{\partial (t - \tau)}[\mathbf{S}(\tau), t - \tau], \quad (12)$$

one obtains that

$$\frac{\partial \mathbf{K}}{\partial \mathbf{S}(\tau)} [\mathbf{S}(\tau), t - \tau] \mathbf{S}'(\tau) = \frac{d}{d\tau} \mathbf{K} [\mathbf{S}(\tau), t - \tau] + \frac{\partial \mathbf{K}}{\partial (t - \tau)} [\mathbf{S}(\tau), t - \tau] . \tag{13}$$

By substituting Eq. (13) into Eq. (11), one has the following:

$$\mathbf{C}(t) = \mathbf{K}[\mathbf{S}(0), t] + \int_0^t \frac{d}{d\tau} \mathbf{K}[\mathbf{S}(\tau), t - \tau] d\tau + \int_0^t \frac{\partial \mathbf{K}}{\partial (t - \tau)} [\mathbf{S}(\tau), t - \tau] d\tau = \mathbf{K}[\mathbf{S}(0), t] + \mathbf{K}[\mathbf{S}(t), 0] - \mathbf{K}[\mathbf{S}(0), t] + \int_0^t \frac{\partial \mathbf{K}}{\partial (t - \tau)} [\mathbf{S}(\tau), t - \tau] d\tau = \mathbf{K}[\mathbf{S}(t), 0] + \int_0^t \frac{\partial \mathbf{K}}{\partial (t - \tau)} [\mathbf{S}(\tau), t - \tau] d\tau.$$
(14)

In summary, Eq. (9) can be rewritten as

$$\mathbf{C}(t) = \mathbf{K}[\mathbf{S}(0), t] + \int_0^t \frac{\partial \mathbf{K}}{\partial \mathbf{S}(\tau)} [\mathbf{S}(\tau), t - \tau] \mathbf{S}'(\tau) d\tau , \qquad (15)$$

or, equivalently, as

$$\mathbf{C}(t) = \mathbf{K}[\mathbf{S}(t), 0] + \int_0^t \frac{\partial \mathbf{K}}{\partial (t - \tau)} [\mathbf{S}(\tau), t - \tau] d\tau.$$
 (16)

2.2. Orthotropic viscoelastic material

First, let us recall that the first, second, and third invariants of $\mathbf{S}(\tau)$ are defined, respectively, as

$$I_1 = \operatorname{tr}(\mathbf{S}), \tag{17}$$

$$I_2 = \frac{1}{2} ((\operatorname{tr}(\mathbf{S}))^2 - \operatorname{tr}(\mathbf{S}^2)), \tag{18}$$

$$I_3 = \det(\mathbf{S}), \tag{19}$$

where we have omitted the dependence of S on τ for convenience. The first invariant is related to the mean normal stress, the second invariant is related to the shear stress, and the third invariant does not appear to have a direct physical meaning. For isotropic materials, the creep kernel can be represented by

$$\mathbf{K}[\mathbf{S}(\tau), t - \tau] = \varphi_1 \mathbf{1} + \varphi_2 \mathbf{S}(\tau) + \varphi_3 \mathbf{S}^2(\tau), \qquad (20)$$

where φ_1 , φ_2 , and φ_3 are scalar functions of the first, second, and third invariants of $\mathbf{S}(\tau)$ reported in Eqs. (17)–(19) and $t-\tau$. We explicitly note that when $\mathbf{S}=\mathbf{0}$, then $\mathbf{K}[\mathbf{0},t-\tau]=\varphi_1\mathbf{1}$. Since we are assuming that $\mathbf{K}[\mathbf{0},s]=\mathbf{1}$ for all s, it follows that φ_1 must be identically equal to 1 when $\mathbf{S}=\mathbf{0}$.

The fourth, fifth, sixth, seventh, and eighth pseudo-invariants of $\mathbf{S}(\tau)$ are defined, respectively, as:

$$I_4 = \mathbf{M} \cdot (\mathbf{SM}), \tag{21}$$

$$I_5 = \mathbf{M} \cdot (\mathbf{S}^2 \mathbf{M}) \,, \tag{22}$$

$$I_6 = \mathbf{N} \cdot (\mathbf{SN}) \,, \tag{23}$$

$$I_7 = \mathbf{N} \cdot (\mathbf{S}^2 \mathbf{N}) \,, \tag{24}$$

$$I_8 = (\mathbf{M} \cdot \mathbf{N})\mathbf{M} \cdot (\mathbf{S}\mathbf{N}), \tag{25}$$

where "." denotes the dot product between vectors, and M and N represent two unit vectors in the reference configuration which define

the axes of anisotropy. For orthotropic materials with two preferred fiber directions, the creep kernel takes the following form [48]:

$$\begin{split} \mathbf{K}[\mathbf{S}(\tau),t-\tau] &= \varphi_1 \mathbf{1} + \varphi_2 \mathbf{S} + \varphi_3 \mathbf{S}^2 + \varphi_4 \mathbf{M} \otimes \mathbf{M} + \varphi_5 (\mathbf{S} \mathbf{M} \otimes \mathbf{M} + \mathbf{M} \otimes \mathbf{S} \mathbf{M}) \\ &+ \varphi_6 \mathbf{N} \otimes \mathbf{N} + \varphi_7 (\mathbf{S} \mathbf{N} \otimes \mathbf{N} + \mathbf{N} \otimes \mathbf{S} \mathbf{N}) + \varphi_8 (\mathbf{M} \otimes \mathbf{N} + \mathbf{N} \otimes \mathbf{M}) \,, \end{split}$$

(26)

where $\varphi_1, \ldots, \varphi_8$ are scalar functions of I_1, \cdots, I_8 and $t - \tau$, and " \otimes " denotes the dyadic tensor product.

Since our experimental data indicate that the vaginal tissue is orthotropic with two (almost) orthogonal families of fibers in the loading directions ($\mathbf{M} \cdot \mathbf{N} = 0$) [25], we propose the use of an orthoropic creep kernel function to describe the tissue's creep behavior. To minimize complexity, we select the following simplified kernel function [49]:

$$\mathbf{K}[\mathbf{S}(\tau), t - \tau] = \varphi_1 \mathbf{1} + \varphi_2 \mathbf{S} + \varphi_4 \mathbf{M} \otimes \mathbf{M} + \varphi_6 \mathbf{N} \otimes \mathbf{N}, \qquad (27)$$

where $\varphi_1=\varphi_1(I_1(\tau),t-\tau)$, $\varphi_2=\varphi_2(I_1(\tau),t-\tau)$, $\varphi_4=\varphi_4(I_4(\tau),t-\tau)$, $\varphi_6=\varphi_6(I_6(\tau),t-\tau)$ are scalar functions of the invariants and pseudo-invariants of $\mathbf{S}(\tau)$ and $t-\tau$, and \mathbf{M} and \mathbf{N} represent the two primary physiological loading directions of the vagina, the LD and CD, respectively.

Based on experimental data, the scalar functions are assumed to have the following forms:

$$\varphi_1 = 1 + \alpha I_1(\tau) \,, \tag{28}$$

$$\varphi_2 = \beta + \gamma(t - \tau) \,, \tag{29}$$

$$\varphi_4 = b_{\infty} \ln(b_r I_4(\tau) + 1) + [(b_0 - b_{\infty}) \ln(b_r I_4(\tau) + 1)] e^{-g_0(t - \tau)}, \tag{30}$$

$$\varphi_6 = c_m \ln(c_r I_6(\tau) + 1) + [(c_0 - c_m) \ln(c_r I_6(\tau) + 1)] e^{-h_0(t - \tau)}, \tag{31}$$

where $\alpha<0$, $\beta>|\alpha|>0$, $\gamma>0$, $b_\infty>b_0>0$, $b_r>0$, $c_\infty>c_0>0$, $c_r>0$, $c_0>0$, and $b_0>0$ are scalar parameters, and $|\alpha|$ denotes the absolute value of α . The exact forms for these scalar functions were selected through a process of trial and error during preliminary modeling attempts. It is worth noting now that these scalar functions are products of time-dependent and stress-dependent functions, resulting in a separable nonlinear viscoelastic model such as the quasi-linear viscoelastic model proposed by Fung for soft tissues [50].

The constitutive relation in Eq. (16) can then be written as

$$\begin{split} \mathbf{C}(t) &= (1+\alpha I_1(t))\mathbf{1} + \beta \mathbf{S} + b_0 \ln(b_r I_4(t) + 1) \mathbf{M} \otimes \mathbf{M} + c_0 \ln(c_r I_6(t) + 1) \mathbf{N} \otimes \mathbf{N} \\ &+ \gamma \int_0^t \mathbf{S}(\tau) d\tau + \Delta b \int_0^t \ln(b_r I_4(\tau) + 1) g_0 e^{-g_0(t-\tau)} \mathbf{M} \otimes \mathbf{M} d\tau \\ &+ \Delta c \int_0^t \ln(c_r I_6(\tau) + 1) h_0 e^{-h_0(t-\tau)} \mathbf{N} \otimes \mathbf{N} d\tau \;, \end{split} \tag{32}$$

with $\Delta b = b_{\infty} - b_0$ and $\Delta c = c_{\infty} - c_0$. Therefore, in order to describe the creep behavior of vaginal tissues, eleven constitutive parameters need to be determined by fitting the model represented in Eq. (32) to experimental data. We explicitly note that when t=0 and restricting $b_0 = c_0 = 0$, after setting $\alpha = -2v/E$ and $\beta = \frac{2(1+v)}{E}$, where E is the Young's modulus and v is the Poisson's ratio, we recover the Kirchhoff-Saint Venant model $\mathbf{E} = \frac{1}{2}(\mathbf{C} - \mathbf{1}) = (\frac{1+v}{E})\mathbf{S} + \frac{v}{E}(\operatorname{tr} \mathbf{S})\mathbf{1}$, where \mathbf{E} is the Lagrangian strain. Furthermore, we note that the specific forms φ_4 and φ_6 are selected to reproduce the typical exponential relationship between stress and strain of soft tissues [51].

3. Model validation

The model was tested using experimental data collected by performing $ex\ vivo$ free-extension inflation creep tests on rat vaginal canals (n=14) [25]. Briefly, the geometrical dimensions of the vaginal specimens were measured under a microscope, then the specimens were mounted

onto concentric needles in a phosphate buffered saline bath and pressurized using a pressure pump. Twenty cycles of preconditioning were applied to each specimen to mitigate subtle variations in tissue stressing resulting from dissection and provide a consistent loading history for each specimen. After preconditioning, each specimen was inflated for three consecutive creep tests, at consecutively increasing constant luminal pressures of 28, 55, and 83 kPa. Inflation during pre-creep, when going from one pressure level to another, occurred at an infusion rate of 0.7 mL/min, and each creep pressure was maintained for 3000 s (50 min) by periodic infusion at a rate of 0.1 mL/min, without recovery between creep tests. Throughout testing, two components of the right Cauchy–Green deformation tensor C ($\hat{C}_{ZZ}(t)$ and $\hat{C}_{\Theta\Theta}(t)$ as defined later), were measured via digital image correlation.

To model the time-dependent deformations arising from the three consecutive creep tests of our experiments, we assume that the luminal pressure history, P(t), is characterized by three linear increases in pressure, each followed by a constant pressure so that

$$P(t) = \begin{cases} P_1 \frac{t}{t_1} & t \in [0, t_1) \\ P_1 & t \in [t_1, t_1^*) \\ P_1 + (P_2 - P_1) \frac{t - t_1^*}{t_2 - t_1^*} & t \in [t_1^*, t_2) \\ P_2 & t \in [t_2, t_2^*) \\ P_2 + (P_3 - P_2) \frac{t - t_2^*}{t_3 - t_2^*} & t \in [t_2^*, t_3) \\ P_3 & t \in [t_3, \infty), \end{cases}$$

$$(33)$$

where P_1 , P_2 , and P_3 represent the three constant pressure values, 28, 55, and 83 kPa, held during the three consecutive creep tests. We note that since the radius and thickness of our specimens changed during creep testing, the Cauchy stress $\sigma(t)$ changed too throughout a creep test. To estimate this Cauchy stress, we consider the loaded vagina to be geometrically equivalent to a capped thin-walled cylindrical pressure vessel without axial forces and in absence of shear. As described elsewhere [52], in an Eulerian cylindrical coordinate system $\{\mathbf{e}_r, \mathbf{e}_\theta, \mathbf{e}_z\}$ with \mathbf{e}_z aligned with the longitudinal axis of the cylinder, σ is represented by

$$\sigma = -P\mathbf{e}_r \otimes \mathbf{e}_r + \frac{Pr}{d}\mathbf{e}_\theta \otimes \mathbf{e}_\theta + \frac{Pr}{2d}\mathbf{e}_z \otimes \mathbf{e}_z , \qquad (34)$$

where P is the value of the luminal pressure, r is the current radius of the vaginal specimen and d is the current thickness. Note that the time dependence is omitted to simplify the notation. As discussed in our experimental study, the average shear strains observed were much smaller than the normal strains in the LD and CD, and thus any shear stresses and strains were neglected for this study. Furthermore, we assume the axial force exerted by the upper needle assembly to be negligible, as its weight was quite small compared to the estimated axial normal forces resulting from inflation [25]. Under these assumptions, we choose to neglect the radial component of the stress, $\sigma_{rr} = -P \approx 0$, since $r \gg d$. In the reference configuration, the average radius, $\bar{r_0}$, and the average thickness, $\bar{d_0}$, were measured to be 2.55 mm and 0.39 mm, respectively. Assuming incompressibility (i.e., $\det(\mathbf{F}) = 1$), the deformation gradient \mathbf{F} is taken to be

$$\mathbf{F} = \lambda_r \mathbf{e}_r \otimes \mathbf{E}_R + \lambda_\theta \mathbf{e}_\theta \otimes \mathbf{E}_\Theta + \lambda_z \mathbf{e}_z \otimes \mathbf{E}_Z$$

= $(\lambda_\theta \lambda_z)^{-1} \mathbf{e}_r \otimes \mathbf{E}_R + \lambda_\theta \mathbf{e}_\theta \otimes \mathbf{E}_\Theta + \lambda_z \mathbf{e}_z \otimes \mathbf{E}_Z$, (35)

where λ_{θ} and λ_{z} describe the stretches in the CD and LD, respectively, and the unit vectors $\{\mathbf{E}_{R},\mathbf{E}_{\Theta},\mathbf{E}_{Z}\}$ define the Lagrangian cylindrical coordinate system, with \mathbf{E}_{Z} aligned with the longitudinal axis of the vagina in the reference configuration. The right Cauchy–Green deformation tensor \mathbf{C} is then

$$\mathbf{C} = (\lambda_{\theta} \lambda_{z})^{-2} \mathbf{E}_{R} \otimes \mathbf{E}_{R} + \lambda_{\theta}^{2} \mathbf{E}_{\Theta} \otimes \mathbf{E}_{\Theta} + \lambda_{z}^{2} \mathbf{E}_{Z} \otimes \mathbf{E}_{Z}. \tag{36}$$

With this assumption on the right Cauchy–Green deformation tensor C, $r=\lambda_{\theta}r_0$ and $d=\lambda_r d_0=(\lambda_{\theta}\lambda_z)^{-1}d_0$ where r_0 and d_0 are the experimentally measured radius and thickness of the vagina in the reference

$$C_{ZZ}(t) = (\lambda_z(t))^2 = \underbrace{1 + \alpha \left(\frac{(\lambda_\theta(t))^2}{\lambda_z(t)} \frac{P(t)r_0}{2d_0} + \lambda_z(t) \frac{P(t)r_0}{d_0} \right) + \beta \frac{(\lambda_\theta(t))^2}{\lambda_z(t)} \frac{P(t)r_0}{2d_0} + b_0 \ln \left(b_r \frac{(\lambda_\theta(t))^2}{\lambda_z(t)} \frac{P(t)r_0}{2d_0} + 1 \right) + elastic contribution}_{\text{elastic contribution}}$$

$$\underbrace{\gamma \int_0^t \frac{(\lambda_\theta(\tau))^2}{\lambda_z(\tau)} \frac{P(\tau)r_0}{2d_0} d\tau + \Delta b \int_0^t \ln \left(b_r \frac{(\lambda_\theta(\tau))^2}{\lambda_z(\tau)} \frac{P(\tau)r_0}{2d_0} + 1 \right) g_0 e^{-g_0(t-\tau)} d\tau}_{\text{elastic contribution}},$$
(39)

$$C_{\Theta\Theta}(t) = (\lambda_{\theta}(t))^{2} = \underbrace{1 + \alpha \left(\frac{(\lambda_{\theta}(t))^{2}}{\lambda_{z}(t)} \frac{P(t)r_{0}}{2d_{0}} + \lambda_{z}(t) \frac{P(t)r_{0}}{d_{0}} \right) + \beta \lambda_{z}(t) \frac{P(t)r_{0}}{d_{0}} + c_{0} \ln \left(c_{r}\lambda_{z}(t) \frac{P(t)r_{0}}{d_{0}} + 1 \right) + \underbrace{\left(\frac{\lambda_{\theta}(t)^{2}}{\lambda_{z}(t)} \frac{P(\tau)r_{0}}{2d_{0}} + \lambda_{z}(t) \frac{P(\tau)r_{0}}{d_{0}} \right) + \beta \lambda_{z}(t) \frac{P(\tau)r_{0}}{d_{0}} + c_{0} \ln \left(c_{r}\lambda_{z}(t) \frac{P(\tau)r_{0}}{d_{0}} + 1 \right) + \underbrace{\left(\frac{\lambda_{\theta}(t)^{2}}{\lambda_{z}(t)} \frac{P(\tau)r_{0}}{d_{0}} \right) + \beta \lambda_{z}(t) \frac{P(\tau)r_{0}}{d_{0}} + c_{0} \ln \left(c_{r}\lambda_{z}(t) \frac{P(\tau)r_{0}}{d_{0}} + 1 \right) + \underbrace{\left(\frac{\lambda_{\theta}(t)^{2}}{\lambda_{z}(t)} \frac{P(\tau)r_{0}}{d_{0}} \right) + \beta \lambda_{z}(t) \frac{P(\tau)r_{0}}{d_{0}} + c_{0} \ln \left(c_{r}\lambda_{z}(t) \frac{P(\tau)r_{0}}{d_{0}} + 1 \right) + \underbrace{\left(\frac{\lambda_{\theta}(t)^{2}}{\lambda_{z}(t)} \frac{P(\tau)r_{0}}{d_{0}} \right) + \beta \lambda_{z}(t) \frac{P(\tau)r_{0}}{d_{0}} + c_{0} \ln \left(c_{r}\lambda_{z}(t) \frac{P(\tau)r_{0}}{d_{0}} + 1 \right) + \underbrace{\left(\frac{\lambda_{\theta}(t)^{2}}{\lambda_{z}(t)} \frac{P(\tau)r_{0}}{d_{0}} \right) + \beta \lambda_{z}(t) \frac{P(\tau)r_{0}}{d_{0}} + c_{0} \ln \left(c_{r}\lambda_{z}(t) \frac{P(\tau)r_{0}}{d_{0}} + 1 \right) + \underbrace{\left(\frac{\lambda_{\theta}(t)^{2}}{\lambda_{z}(t)} \frac{P(\tau)r_{0}}{d_{0}} \right) + \beta \lambda_{z}(t) \frac{P(\tau)r_{0}}{d_{0}} + c_{0} \ln \left(c_{r}\lambda_{z}(t) \frac{P(\tau)r_{0}}{d_{0}} + 1 \right) + \underbrace{\left(\frac{\lambda_{\theta}(t)^{2}}{\lambda_{z}(t)} \frac{P(\tau)r_{0}}{d_{0}} \right) + \beta \lambda_{z}(t) \frac{P(\tau)r_{0}}{d_{0}} + c_{0} \ln \left(c_{r}\lambda_{z}(t) \frac{P(\tau)r_{0}}{d_{0}} + 1 \right) + \underbrace{\left(\frac{\lambda_{\theta}(t)^{2}}{\lambda_{z}(t)} \frac{P(\tau)r_{0}}{d_{0}} + 1 \right) + \underbrace{\left(\frac{\lambda_{\theta}(t)^{2}}{\lambda_{z}(t)} \frac{P(\tau)r_{0}}{d_{0}} \right) + \frac{\lambda_{z}(t)^{2}}{\lambda_{z}(t)^{2}} + \underbrace{\left(\frac{\lambda_{\theta}(t)^{2}}{\lambda_{z}(t)} \frac{P(\tau)r_{0}}{d_{0}} + 1 \right) + \underbrace{\left(\frac{\lambda_{\theta}(t)^{2}}{\lambda_{z}(t)} \frac{P(\tau)r_{0}}{d_{0}} \right) + \underbrace{\left(\frac{\lambda_{\theta}(t)^{2}}{\lambda_{z}(t)}$$

Box I.

configuration, respectively. Then, the Cauchy stress in Eq. (34) can be re-written as

$$\sigma = \lambda_{\theta}^{2} \lambda_{z} \frac{P r_{0}}{d_{0}} \mathbf{e}_{\theta} \otimes \mathbf{e}_{\theta} + \lambda_{\theta}^{2} \lambda_{z} \frac{P r_{0}}{2 d_{0}} \mathbf{e}_{z} \otimes \mathbf{e}_{z},$$
(37)

and, since $\mathbf{S} = J\mathbf{F}^{-1}\sigma\mathbf{F}^{-T}$, the second Piola–Kirchhoff stress can be expressed as

$$\mathbf{S} = \lambda_z \frac{Pr_0}{d_0} \mathbf{E}_{\Theta} \otimes \mathbf{E}_{\Theta} + \frac{\lambda_{\theta}^2}{\lambda_z} \frac{Pr_0}{2d_0} \mathbf{E}_Z \otimes \mathbf{E}_Z . \tag{38}$$

After assuming that $\mathbf{M}=\mathbf{E}_Z$ and $\mathbf{N}=\mathbf{E}_\Theta$ and given the second Piola–Kirchhoff stress in Eq. (38), the constitutive equation in Eq. (32) is expressed as a set of nonlinear implicit equations in $\lambda_z(t)$ and $\lambda_\theta(t)$. Specifically, the components $C_{ZZ}(t)$ and $C_{\Theta\Theta}(t)$ of the right Cauchy–Green deformation tensor are (see Box I). We note that the dependence of C_{ZZ} , $C_{\Theta\Theta}$, P, λ_z , and λ_θ on time is reintroduced in the given equations.

This set of nonlinear equations can be solved numerically to find $\lambda_z(t)$ and $\lambda_\theta(t)$, and therefore $C_{ZZ}(t)$ and $C_{\Theta\Theta}(t)$, at any time t over the entire pressure history defined in Eq. (33) once the pressure values, P_1 , P_2 , and P_3 , are given, assuming that $\lambda_z(0)=1$ and $\lambda_\theta(0)=1$, and that the constitutive parameters, α , β , γ , b_0 , b_r , Δb , c_0 , c_r , Δc , g_0 , h_0 , the initial radius r_0 and thickness d_0 of each specimen are known.

For determining the best fit model parameters for each tested vaginal specimen (n=14), the square of the residual, χ , defined as the difference between the theoretically calculated right Cauchy–Green deformation components, $C_{ZZ}(t)$ and $C_{\Theta\Theta}(t)$, and the corresponding experimentally measured right Cauchy–Green deformation components, $\hat{C}_{ZZ}(t)$ and $\hat{C}_{\Theta\Theta}(t)$, was minimized. More specifically, the following function:

$$\chi^{2} = \sum_{t=1}^{N} (\hat{C}_{ZZ}(t) - C_{ZZ}(t))^{2} + (\hat{C}_{\Theta\Theta}(t) - C_{\Theta\Theta}(t))^{2},$$
(41)

was minimized using the trust-region-reflective nonlinear least squares regression algorithm of the MATLAB (R2023a, Mathworks, Natick, MA) function lsqnonlin under the default settings. In Eq. (41), N is the number of experimental data points collected from each specimen from the first pre-creep test to the third creep test. The theoretical right Cauchy–Green deformation components, $C_{ZZ}(t)$ and $C_{\Theta\Theta}(t)$, were computed by considering the loading history in Eq. (33). The pressures P_1 , P_2 , and P_3 in Eq. (33) were determined by averaging the experimentally measured constant pressure throughout the duration of each creep test, and the transition times t_1 , t_1^* , t_2 , t_2^* , and t_3 were taken as the first or last time points for which the experimental pressure fell within certain bounds (< 5%) of the aforementioned mean creep pressures.

This approach was used, rather than directly using the experimental pressure data, because of the periodic sawtooth pressure waves that were inevitably generated when trying to maintain constant pressures during creep tests [25].

This fitting procedure was repeated multiple times with random sets of initial guesses for the initial constitutive parameters. Different initial guesses led to different resulting values for the fitted constitutive parameters, likely due to the presence of various local minima of the squared residual in Eq. (41). The set of parameters which resulted in the lowest value of the correlation coefficient, R^2 , defined as:

$$R^{2} = 1 - \frac{\chi^{2}}{\sum_{t=1}^{N} [(\hat{C}_{\Theta\Theta}(t) - \hat{\mu})^{2} + (\hat{C}_{ZZ}(t) - \hat{\mu})^{2}]},$$
(42)

where $\hat{\mu} = \frac{1}{2N} \sum_{t=1}^{N} (\hat{C}_{ZZ}(t) + \hat{C}_{\Theta\Theta}(t))$ represents the mean of the experimental right Cauchy–Green deformation components, was selected to be the best fit model parameters. As an additional measure of fit quality, the normalized root mean square error, ϵ , defined as

$$\epsilon = \frac{\chi^2}{\sum_{i=1}^{N} (\hat{C}_{ZZ}(t)^2 + \hat{C}_{\Theta\Theta}(t)^2)},$$
(43)

was calculated for each specimen.

For fitting, the possible values for α and β were restricted such that the corresponding values of E and ν , as per the aforementioned simplification to the Kirchhoff-Saint Venant model following Eq. (32), had values between 0 and 100 GPa and 0 and 0.5, respectively. The other nine parameters were set to be: $0 \le b_0 \le 0.1$, $0 \le b_r \le 3$ [kPa⁻¹], $0 \le \Delta b \le 0.05$, $0 \le g_0 \le 0.4$ [s⁻¹], $0 \le c_0 \le 0.2$, $0 \le c_r \le 0.4$ [kPa⁻¹], $0 \le \Delta c \le 0.05$, $0 \le h_0 \le 0.4$ [s⁻¹], $0 \le \gamma \le 0.02$ [kPa s)⁻¹].

Once the parameters were obtained for each specimen, paired ttests were used to compare the differences between parameters that describe the pre-creep and creep behavior in the LD and CD via C_{ZZ} and $C_{\Theta\Theta}$ in Eqs. (39)-(40). Specifically, a paired t-test was used to compare parameters b_0 and c_0 , b_r and c_r , Δb and Δc , and g_0 and h_0 . The values for b_0 and c_0 were normally distributed under Ryan-Joiner test with no outliers. The values for b_r and c_r were not normally distributed under Ryan-Joiner test, each with a single outlier under Grubb's test. A $log_{10}(x)$ transformation was performed to normalize the data. While the values for Δb were not normally distributed, the values for Δc were, with both data sets having no outliers. Likewise, the values for g_0 were not normally distributed while the values for h_0 were, both with no outliers. For both parameter pairs (Δb and Δc , g_0 and h_0), a $log_{10}(x)$ transformation was performed to normalize the data. All statistical comparisons were performed in Minitab 21 (Minitab, Inc., Version 20.3, State College, PA), with statistical significance for t-tests

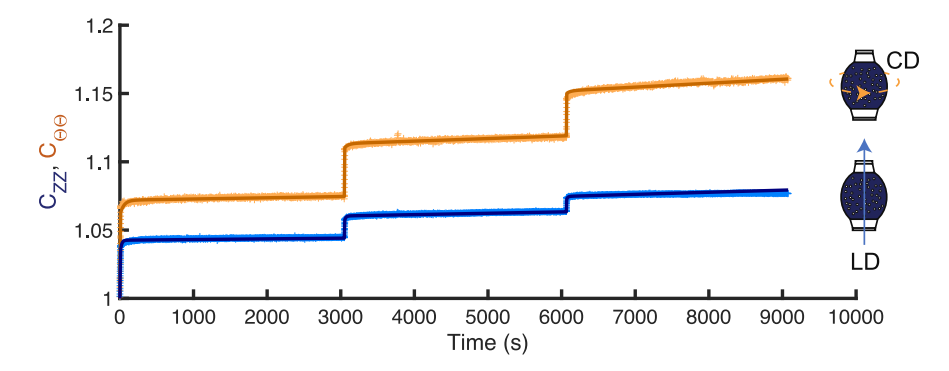


Fig. 1. Components C_{ZZ} and $C_{\Theta\Theta}$ of the right Cauchy–Green deformation tensor C over time t during three pre-creep and creep tests at 27.23 kPa, 54.74 kPa, and 82.37 kPa for one representative specimen. The dimensions of the representative specimen were $r_0 = 2.996$ mm and $d_0 = 0.40$ mm, and the transition times were $t_1 = 11.5$ s, $t_1^* = 3049$ s, $t_2 = 3055$ s, $t_2^* = 6064.7$ s, and $t_3 = 6070.2$ s. Model fit (continuous lines) and experimental data (+ symbols) are shown in blue for C_{ZZ} and in orange for $C_{\Theta\Theta}$. The value of the best fit parameters for this specimen, specimen f, are reported in Table 1. (For interpretation of the references to color in this figure legend, the reader is referred to the web version of this article.)

set to p < 0.05. Any data sets with a p < 0.1 under Ryan-Joiner test were considered to be violating assumptions of normality for the sake of statistical comparisons. When relevant, statistical comparisons were performed on both original and transformed data sets, and all transformed data were confirmed to be normalized under Ryan-Joiner test with no outliers. Not all comparisons which indicated statistical significance in transformed data sets also indicated statistical significance in the corresponding original data sets, and results for both statistical comparisons are reported for such cases. Otherwise, results are reported for statistical comparisons as performed on the transformed data only.

The means of the fitting parameters, denoted by $\bar{\alpha}$, $\bar{\beta}$, $\bar{\gamma}$, \bar{b}_0 , \bar{b}_r , $\bar{\Delta}b$, \bar{g}_0 , \bar{c}_0 , \bar{c}_r , $\bar{\Delta}c$, or \bar{h}_0 , were used in combination with physical dimensions $(r_0=2.984 \text{ mm}, d_0=0.41 \text{ mm})$, transition times $(t_1=8 \text{ s}, t_1^*=3040.9 \text{ s}, t_2=3045.4 \text{ s}, t_2^*=6075.1 \text{ s},$ and $t_3=6079.1 \text{ s})$, and pressure values $(P_1=27.59 \text{ kPa}, P_2=55.39 \text{ kPa},$ and $P_3=83.37 \text{ kPa})$ associated with one representative specimen to determine the effect of each constitutive parameters on the components $C_{ZZ}(t)$ and $C_{\Theta\Theta}(t)$ of the right Cauchy–Green deformation tensor. Toward this end, Eqs. (39)–(40) were solved using the default trust-region-dogleg algorithm of MATLAB's fsolve function several times, with a function tolerance of 1×10^{-12} , varying one of the eleven constitutive parameters around its mean value while keeping all the other constitutive parameters fixed at their mean values. The varied parameter was multiplied by a set of four scalar values, with the exact scalar values selected to generate differences in the curves representing $C_{ZZ}(t)$ and $C_{\Theta\Theta}(t)$.

4. Results

Fig. 1 displays the results of fitting the constitutive model to experimental data for one representative specimen, subjected to consecutive luminal pressures of 27.23 kPa, 54.74 kPa, and 82.37 kPa for the three consecutive creep tests. The dimensions of the representative specimen were $r_0 = 2.996$ mm and $d_0 = 0.40$ mm, and the transition times were $t_1 = 11.5$ s, $t_1^* = 3049$ s, $t_2 = 3055$ s, $t_2^* = 6064.7$ s, and $t_3 = 6070.2$ s. The model accurately captured the overall vaginal tissue response to three consecutive creep tests, with the theoretically predicted components of the right Cauchy-Green deformation tensor close to the experimental values across the full loading history. Fig. 2 presents magnified views of the same fit which better show the effectiveness of the model in capturing the pre-creep and creep behavior for the representative specimen. The greatest deviations of the model from the experimental data generally occurred during the first pre-creep (Fig. 2(A)), as the predicted tissue's compliance was more nonlinear than what was observed experimentally. These differences between the model fit and the experimental data were not present during the second and third pre-creep tests (Fig. 2(C) and (E)).

Table 1 reports the values of the model parameters that provided the best fit to the experimental data for three consecutive tests. The normalized root mean square error, ϵ , and correlation coefficient, R^2 , for the set of data collected from each specimen, as well as the mean and standard error of the mean (S.E.M.) for each parameter across all specimens (n = 14) are also reported. Each fit had ϵ values below 0.06, and R^2 values close to one for each specimen.

Fig. 3 compares four pairs of calculated direction-specific parameters of the model: b_0 and c_0 , b_r and c_r , Δb and Δc , and g_0 and h_0 . Paired t-tests revealed statistically significant differences between three of the four pairs. The parameters b_0 , and c_0 , which dictate the elastic response of the tissue in the LD and CD, respectively, were found to be statistically different. Specifically, the parameter c_0 was significantly greater than b_0 (p = 0.001), indicating that the tissue in the CD is overall more compliant than in the LD. The average value for b_r was greater than the average value for c_r , and this difference suggests that the elastic behavior in the LD is more nonlinear than in the CD. These results were statistically significant for the normalized data (p < 0.001) under paired t-tests, but they were not significant under paired t-test for the original data set (p = 0.054). The parameters, Δc and Δb , which define the short-term creep magnitude, were not significantly different (p = 0.913). The short-term creep rate parameters relative to the LD, g_0 , were significantly higher (p = 0.004) than the corresponding parameters relative to the CD, h_0 .

Figs. 4–5 demonstrate the effect of each constitutive parameter on $C_{\Theta\Theta}(t)$ in Eq. (40). As mentioned earlier, the values for all parameters are fixed to be equal to the mean values reported in Table 1, except for the individual parameter being varied, as noted in the legends of the figures. For the sake of brevity, only the effects of α , β , c_0 , c_r , γ , Δc , and h_0 on $C_{\Theta\Theta}(t)$ are shown. Parameters such as α , β , and γ , which appeared in both Eqs. (39) and (40) had very similar effects on $C_{ZZ}(t)$ and $C_{\Theta\Theta}(t)$, while parameters that only appeared in $C_{ZZ}(t)$ in Eq. (39) such as b_0 , b_r , Δb , and g_0 had correspondingly identical effects as parameters that appeared only in $C_{\Theta\Theta}(t)$ (e.g., g_0 affected $C_{ZZ}(t)$ in a similar way as h_0 affected $C_{\Theta\Theta}(t)$). Moreover, the parameters that appeared only in $C_{ZZ}(t)$ had minimal effects on the deformations in the CD, and vice versa. As such, figures presenting the effects of the constitutive parameters on $C_{ZZ}(t)$, and figures presenting the effects of b_0 , b_r , Δb , and g_0 on $C_{\Theta\Theta}(t)$ are not shown here.

In our model, the elastic portions of the scalar functions φ_1 and φ_2 describe isotropic linear increase stretch-stress behavior (Eqs. (28)–(29)). The elastic parameter β within φ_2 (Eq. (28)) affects only the directions in which stresses are applied (Eq. (32)). Since β is restricted to be positive, this results in linear increases in normal strains with applied normal stresses. Conversely, the elastic parameter α within φ_1 is multiplied by the first stress invariant (Eq. (28)), which is the trace of the stress (Eq. (17)). Since α is restricted to be negative by

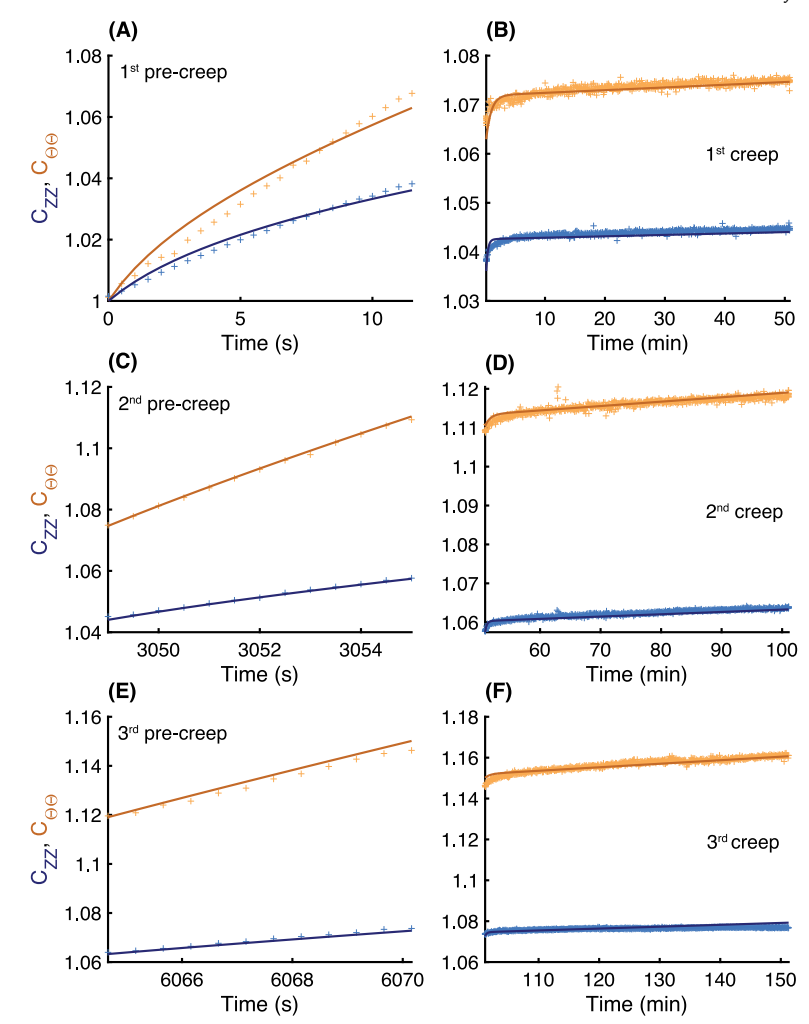


Fig. 2. Zoomed in view of the components C_{ZZ} and $C_{\Theta\Theta}$ of the right Cauchy–Green deformation tensor C over time t during (A), (C), (E) pre-creep tests and (B), (D), (F) creep tests at 27.23 kPa, 54.74 kPa, and 82.37 kPa luminal pressures for the representative specimen shown in Fig. 1. The dimensions of the representative specimen were $t_0 = 2.996$ mm and $d_0 = 0.40$ mm, and the transition times were $t_1 = 11.5$ s, $t_1^* = 3049$ s, $t_2 = 3055$ s, $t_2^* = 6064.7$ s, and $t_3 = 6070.2$ s. Model fit (continuous lines) and experimental data (+ symbols) are shown in blue for C_{ZZ} and in orange for $C_{\Theta\Theta}$. The value of the best fit parameters for this specimen, specimen f, are reported in Table 1. (For interpretation of the references to color in this figure legend, the reader is referred to the web version of this article.)

our constitutive assumptions, any positive normal stress applied in any direction results in some compressive normal strain in all directions. This represents a degree of strain coupling, or what may otherwise be referred to as Poisson effects. However, since β is restricted to be greater than the absolute value of α , positive strains will always result in the directions of an applied normal stress, assuming the normal stresses applied in other loading directions do not greatly exceed it.

Fig. 4(A)–(B), (E)–(F), and (I)–(J) demonstrate the effect of varying parameters α and β on the resulting stretch in the CD during precreep (elastic) portion of one representative experiment. Increasing α (Fig. 4(A), (E), and (I)) decreases the amount of deformation observed in the CD, while increasing β (Fig. 4(B), (F), and (J)) increases the amount of deformation observed in a complementary manner. However, the magnitude for the obtained values for α and β were small compared to the other direction-specific elastic parameters (b_0 , b_r , c_0 , c_r , Table 1), and as such, the parameters' values must be increased by several orders of magnitude in order to induce variations in the deformation vs. time curves which are comparable to the effects of varying the other elastic parameters by much smaller amounts.

Conversely to the linear elastic relationships of φ_1 and φ_2 , the elastic portions of φ_4 and φ_6 describe direction-specific logarithmic increases in stretch with normal stress (Eqs. (30)–(31)). In particular, φ_4 scales only with normal stresses in the LD and results in normal strains in the LD, and φ_6 likewise scales with normal stresses and results in

normal strains in the CD (Eq. (32)). Within φ_4 and φ_6 , the elastic parameters b_0 and c_0 control the magnitude of these scalar functions to the stretch. Since the elastic parameters b_r and c_r lie inside of the natural logarithms, they control the relative rate of logarithmic growth of stretch with applied normal stress. Fig. 4(C)–(D), (G)–(H), and (K)–(L) demonstrate the effect of varying the parameters c_0 and c_r on the resulting stretch in the CD during pre-creep (elastic) portion of a representative experiment. Increasing c_0 (Fig. 4(C), (G), and (K)) increases the total deformation seen without radically altering the relative shape of the overall deformation vs. time curves. Conversely, increasing c_r (Fig. 4(D), (H), and (L)) both increases the total stretch seen and alters the shape of the pre-creep curve, with higher c_r values resulting in a more nonlinear deformation vs. time curve.

Just as the elastic portions of the scalar functions φ_1 and φ_2 describe an isotropic behavior for pre-creep which scales linearly with stress, the viscoelastic portion of the scalar function φ_2 describes an isotropic behavior for creep (Eq. (29)) which scales linearly with applied stress and with time (Eq. (32)). Conversely, the viscoelastic contributions of φ_4 and φ_6 define the nonlinear direction-specific creep behaviors (Eqs. (30)–(31)), with φ_4 scaling with normal stresses and causing normal strains in the LD, and φ_6 scaling with normal stresses and causing normal strains in the CD (Eq. (32)). The scalar functions φ_4 and φ_6 introduce a logarithmic dependence on stress and an exponential dependence on time. As such, they define the short-term stretching

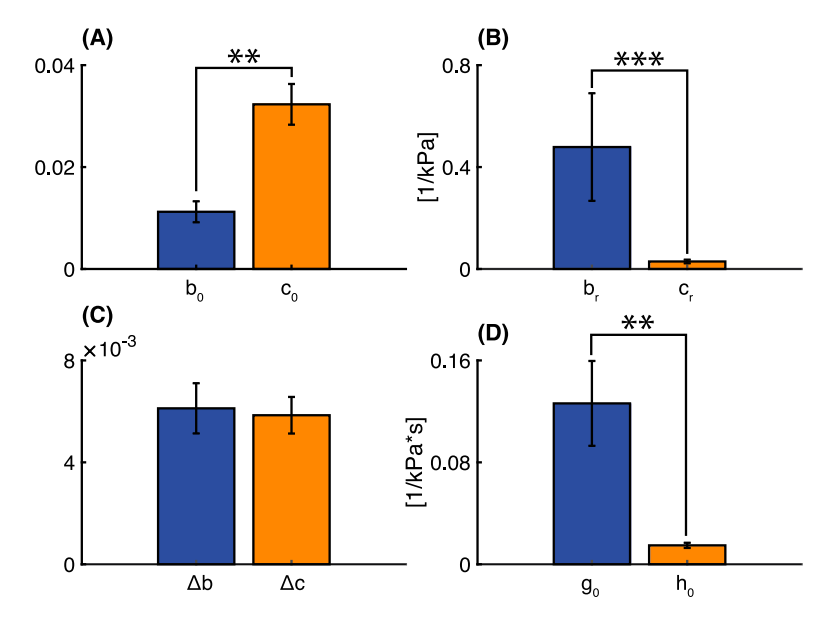


Fig. 3. Comparisons between the four pairs of direction-specific parameters (A) b_0 and c_0 , (B) b_r and c_r , (C) Δb and Δc , and (D) g_0 and h_0 . Parameters that affect the mechanical response in the LD are in blue, while those that affect the mechanical response in the CD are in orange. Under paired t-test, there were statistically significant differences (**p < 0.01, ****p < 0.001) between three of the four sets of parameters after normalizing transformations. (For interpretation of the references to color in this figure legend, the reader is referred to the web version of this article.)

rate during creep, which we have previously termed as primary creep, while φ_2 defines the stretching rate after primary creep, which we have described as secondary creep (Eq. (32)). The viscoelastic parameter γ within φ_2 (Eq. (29)) is multiplied by the applied stress (Eq. (32)), and thus defines the secondary creep rate in both loading directions. The viscoelastic parameters Δb and Δc from φ_4 and φ_6 (Eqs. (30)–(31)) lie outside the time integrals (Eq. (32)), and thus directly define the magnitude of primary creep in the LD and CD, respectively. The parameters g_0 and h_0 (Eqs. (30)–(31)) appear in the exponent of exponential functions, and thus define the rates at which primary creep occurs in the LD and CD.

The effects of γ , Δc , and h_0 on the resulting deformation in the CD can be seen in Fig. 5. Increasing γ (Fig. 5(A), (E), and (I)) increases the secondary creep rate, and thus the amount of stretch which occurs during each creep test. Increasing Δc (Fig. 5(B), (F), and (J)) increases the amount of stretch seen during primary creep, without affecting the relative shape of the overall stretch vs. time curve during creep. Conversely, increasing h_0 (Fig. 5(C), (G), and (K)) does not notably affect the overall amount of stretch during creep, but more importantly changes the shape of the stretch vs. time curve. This effect is most noticeable in the first few hundred seconds of each creep test, as can be seen in Fig. 5(D), (H), and (L), which provides a magnified view of the first part of each creep test.

5. Discussion

This study presents the first constitutive model that describes the creep behavior of vaginal tissue under a state of plane stress. The proposed viscoelastic model, which accounts for the nonlinearity, anisotropy, and finite deformations of the tissue, was validated against experimental data previously collected from free-extension inflation tests on rat vaginal specimens [25]. For the duration of three consecutive creep tests, including the pre-creep tests, the constitutive model closely captured the overall experimental behavior of vaginal tissue in both the LD and CD (Figs. 1 and 2), with high correlation coefficient values and low normalized root mean square error values (Table 1).

In the proposed model, we assumed that the vaginal tissue behaves as a separable nonlinear viscoelastic material. This assumption was made when selecting the scalar functions φ_1 , φ_2 , φ_4 , and φ_6 in Eq. (27) to be the products of functions of time alone and functions of stress

alone. This assumption was also made in a published study by Peña et al. [21] on the stress relaxation of prolapsed human vaginal tissue. However, our experiments, as well as the experiments conducted by Peña et al. were not optimally designed for discerning nonlinearities in the viscoelasticity of vaginal tissue. In particular, our free-extension inflation experiments did not include a recovery period between consecutive creep tests at various pressure values, while Pena et al. only compared normalized stress relaxation data at stretches of 1.3 and 1.4. Further creep (and stress relaxation) experiments that incorporate recovery periods and are conducted at largely different values of applied stress (and strain) should be performed to fully characterize and model the viscoelastic behavior of vaginal tissue.

The anisotropic behavior of vaginal tissue was determined by direction-specific constitutive parameters, notably those denoted as b_0 , b_r , Δb , and g_0 in the LD and c_0 , c_r , Δc , and h_0 in the CD (refer to Eqs. (39)-(40)). Statistical analyses on the (normalized) data sets revealed that three of the four direction-specific parameters exhibited significant differences (Fig. 3). Each vaginal specimen was more compliant in the CD, as indicated by the greater values of c_0 compared to b_0 (Fig. 3(A)). The elastic behavior of most specimens was more nonlinear in the LD than the CD, reflected by the greater values of b_r compared to c_r (Fig. 3(B)). While the values of b_r were not significantly greater than the values of c_r for the original data under paired t-test, this was likely a result of the statistical distribution of the data, as the difference was significant for the normalized data set. There were no significant differences between Δb and Δc , the parameters that control the initial increases in strain during each creep test (Fig. 3(C)). While our previous experimental study did note that more primary creep occurred in the CD than the LD through all three creep tests [25], the amount of primary creep which occurs is not flatly determined by the constitutive parameters Δb and Δc . Rather, the amount of primary creep in each direction is a byproduct of the relevant parameter (Δb or Δc) and the magnitude of applied stress in that direction. Thus, our theoretical findings do not contradict our experimental findings, but rather suggest that the amount of primary creep in the two directions may be similar if equibiaxial stress were to be applied. Finally, the primary creep rate parameter in the LD, go, was far greater than the corresponding parameter in the CD, h_0 , indicating that primary creep occurred more quickly in the LD than in the CD (Fig. 3(D)). The higher primary creep

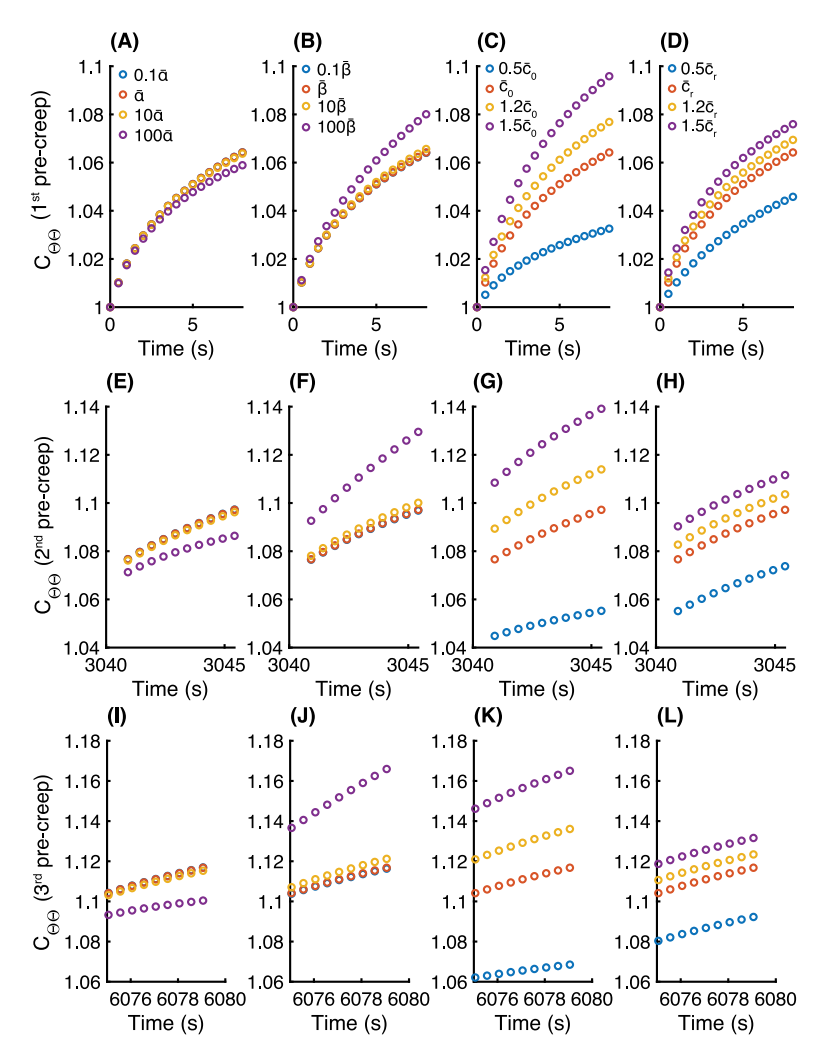


Fig. 4. Effect of α , β , c_0 , and c_r on the component $C_{\Theta\Theta}$ of the right Cauchy–Green deformation tensor during (A)–(D) first pre-creep, (E)–(H) second pre-creep, and (I)–(L) third pre-creep. The parameters $\bar{\alpha}$, $\bar{\beta}$, \bar{c}_0 , and \bar{c}_r are the mean values of α , β , c_0 , and c_r reported in Table 1. Changes in α for (A), (E), and (I) are reported in (B), changes in β for (B), (F), and (J) are reported in (B), changes in c_0 for (C), (G), and (K) are reported in (C), and changes in c_0 for (D), (H), and (L) are reported in (D). (For interpretation of the references to color in this figure legend, the reader is referred to the web version of this article.)

rate in the LD may result from a greater amount of collagen fibers in the LD [53], which may also be the cause of significant differences between b_r and c_r .

A quirk of our model is that, theoretically, the terms that describe the isotropic elastic response, which are the α -term and the β -term in Eq. (32), could dominate as the stress draws closer to infinity since the contributions from direction-specific terms, the b_0 -term and the c_0 -term, which contain natural logarithms, would increase at a much slower rate. This contradicts experimental evidence that seems to suggest that the vaginal tissue behaves more as an isotropic material at low stresses and strains while it becomes more anisotropic at higher stresses and strains [54]. However, the numerical values of α and β were determined to be several order of magnitude smaller than the numerical values of the direction-specific parameters when curve-fitting our experimental data (Table 1). Thus, the α -term and β -term had a negligible effect on the overall mechanical behavior of the vaginal tissue (Fig. 4(A)-(B), (E)–(F), (I)–(J)) compared to the direction-specific parameters (Fig. 4(C)-(D), (G)-(H), (K)-(L)). Since rat vaginal tissue ruptures at stresses not much higher than the applied stresses of our creep experimental study [55], we expect that our model would still be able to capture the anisotropic response of the tissues at these higher stresses.

Our constitutive model has a viscoelastic term, the γ -term in Eq. (32) that contributes to the mechanical response in both the LD and CD, and two viscoelastic terms, the Δb -term and the Δc -term, which are

specific to the loading directions. These terms improved the fidelity of our model with regards to the experimental results since they captured the differences between primary and secondary creep in vaginal tissue. Specifically, in our previous experimental study [25], we observed that strain increased logarithmically over time during primary creep and linearly over time during secondary creep, with the primary creep rates decreasing and the secondary creep rates increasing with the applied pressure from the first to the third creep test. In the proposed model, the γ -term described the shared steady-state linear secondary creep behavior (Fig. 5(A), (E), (I)) while the direction-specific viscoelastic terms were introduced to reproduce the primary creep behavior (Fig. 5(B)–(D), (F)–(H), (J)–(L)). The use of multiple viscoelastic terms in constitutive models of soft tissues is very common. For example, Peña et al. proposed the use of four viscoelastic terms for describing the stress relaxation of vaginal tissue with a transversely isotropic model, two each for the matrix and fibers [21]. The need for multiple viscoelastic terms in constitutive models for vaginal tissue possibly suggests that there may be multiple micro-structural mechanisms which dictate the overall viscoelastic behavior of this tissue.

To the best of our knowledge, this study represents the first effort at modeling the time-dependent strain response of vaginal tissue subjected to biaxial loading instead of uniaxial loading. For simplicity, due to the lack of experimental data to model the response of the tissue along the radial direction (RD), we assumed that $\mathbf{C}(t)$ reduced to a linear

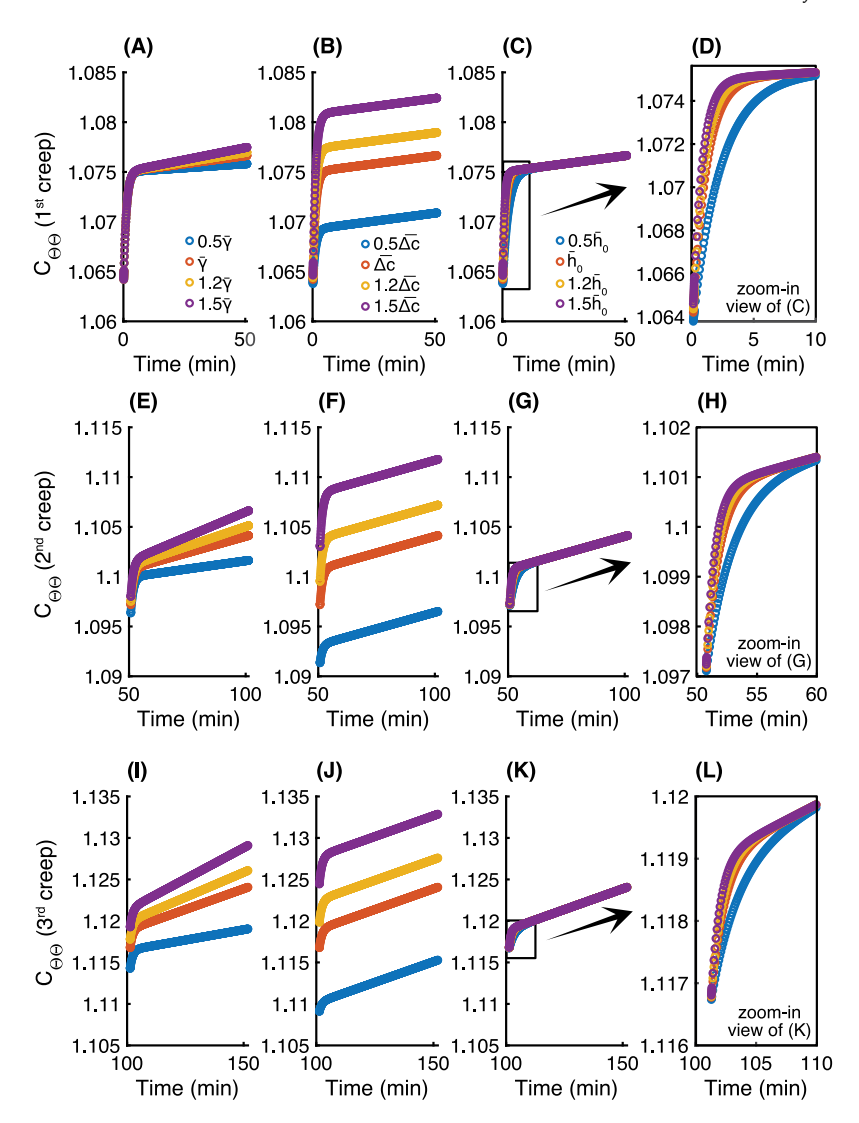


Fig. 5. Effect of γ , Δc , and h_0 on the component $C_{\Theta\Theta}$ of the right Cauchy–Green deformation tensor during (A)–(D) first creep, (E)–(H) second creep, and (I)–(L) third creep. The parameters $\bar{\gamma}$, $\bar{\Delta} c$, and \bar{h}_0 are the mean values of γ , Δb , and h_0 reported in Table 1. Changes in γ for (A), (E), and (I) are reported in (A), changes in Δc for (B), (F), and (J) are reported in (B), and changes in h_0 for (C)–(D), (G)–(H), and (K)–(J) are reported in (C). (For interpretation of the references to color in this figure legend, the reader is referred to the web version of this article.)

function solely dependent on S(t) in the RD, without the inclusion of additional viscoelastic terms (Eq. (32)). It is conceivable that other elastic or viscoelastic terms might be necessary to ensure the accurate representation of the mechanical response of the tissue in the RD within our constitutive model. Notably, in estimating the thickness d of each specimen in the current configuration from their measured value d_0 in the reference configuration, we also assumed incompressibility (Eq. (35)). However, this assumption was not strictly enforced on the right Cauchy–Green deformation tensor during our curve fitting, posing a significant limitation to our study. It could potentially be enforced by requiring that the component $C_{RR}(t)$ of the right Cauchy–Green deformation tensor, expressed as

$$C_{RR}(t) = 1 + \alpha \left(\frac{(\lambda_{\theta}(t))^2}{\lambda_z(t)} \frac{P(t)r_0}{2d_0} + \lambda_z(t) \frac{P(t)r_0}{d_0} \right) , \tag{44} \label{eq:cross}$$

satisfies $\det(\mathbf{C}) = 1$. This would place restrictions on the values of α , the only parameter directly appearing in Eq. (44). In this study, we neglected Eq. (44) since we had no information on the compressibility of vaginal tissue or pre-creep and creep data in the RD. Variations in thickness of vaginal tissue during biaxial testing will need to be experimentally monitored in future using techniques such as optical coherence tomography, as done in our recent study on uterosacral

ligaments [56]. Alternatively, measuring the overall volume of the organ during pre-creep and creep could provide insights into whether the vagina is incompressible and allow for estimates of $C_{RR}(t)$ following Treloar's approach for rubbers [57].

We agree with the sentiment expressed by the famous quote attributed to John von Neumann (1903–1957): "With four parameters I can fit an elephant, and with five I can make him wiggle his trunk". Hence, we tried our very best to maintain simplicity in our constitutive model and minimize the number of parameters. Despite our efforts, our final constitutive relation required the determination of eleven constitutive parameters to fit experimental data of vaginal tissue in two directions at three pre-creep and creep tests (Eq. (32)). We do not rule out the possibility that a constitutive model with a reduced number of parameters may also viable. For example, as we discussed above, the contributions of the parameters α and β to the overall mechanical behavior were almost negligible. Thus, one could fit our experimental data with a constitutive model that does not include the α -term in Eq. (28) and β -term in Eq. (29). However, the omission of these terms would prevent us from recovering the Kirchhoff-Saint Venant model.

The proposed model effectively characterized the *ex vivo* mechanical response of vaginal tissue to three consecutive pre-creep and creep tests (Figs. 1–2). However, the predictive capabilities of the model,

Table 1Best-fit model parameters, correlation coefficients R^2 , and normalized root mean square errors ϵ for each vaginal specimen (a to n), as well as their mean values and standard error of the mean (S.E.M.) values across all specimens (n = 14).

Specimen	b_0	b_r [kPa ⁻¹]	Δb	$g_0 [s^{-1}]$	α [kPa ⁻¹]	β [kPa ⁻¹]	γ [(kPa·s) ⁻¹]
a	0.01909	0.1152	0.00579	0.0203	-1.443E-05	6.970E-05	2.799E-09
b	0.00496	0.6858	0.01493	0.2936	-2.963E-05	8.895E-05	2.761E-09
c	0.01538	0.1144	0.00521	0.0261	-2.597E-05	1.022E-04	3.969E-09
d	0.00128	1.6372	0.00904	0.2805	-4.124E-06	1.513E-05	2.158E-09
e	0.00844	0.0823	0.00431	0.1812	-3.054E-07	3.289E-05	1.412E-09
f	0.01844	0.0447	0.00562	0.0609	-7.599E-05	2.280E-04	4.325E-09
g	0.02688	0.0307	0.00413	0.0126	-2.608E-08	8.195E-08	2.527E-09
h	0.01742	0.0932	0.00336	0.0038	-4.339E-07	3.899E-05	1.275E-09
i	0.01185	0.0715	0.00178	0.0328	-8.813E-07	4.065E-05	2.3364E-09
j	0.00713	0.3394	0.00591	0.1772	-3.529E-05	1.062E-04	2.248E-09
k	0.00275	0.4221	0.00893	0.2027	-4.811E-05	1.443E-04	2.815E-09
1	0.00024	2.7907	0.01107	0.3760	-6.014E-08	2.498E-07	4.272E-09
m	0.01109	0.1652	0.00374	0.0853	-1.463E-05	8.632E-05	2.628E-09
n	0.01219	0.1075	0.00197	0.0149	-4.553E-08	7.612E-05	6.728E-10
Mean	0.01122	0.4786	0.00612	0.1263	-1.785E-05	7.355E-05	2.586E-09
S.E.M.	0.00198	0.2035	0.00095	0.0321	5.919E-06	1.586E-05	2.769E-10
Specimen	c_0	c_r [kPa ⁻¹]	Δc	$h_0 [s^{-1}]$		R^2	ϵ
a	0.02637	0.0207	0.00930	0.00679		0.9974	0.05101
b	0.02962	0.1020	0.00508	0.00589		0.9990	0.03205
c	0.02785	0.0662	0.00802	0.00765		0.9991	0.02989
d	0.05718	0.0086	0.00668	0.01577		0.9982	0.04190
e	0.03999	0.0137	0.00365	0.02464		0.9989	0.03242
f	0.01833	0.0336	0.00486	0.01932		0.9994	0.02446
g	0.04914	0.0086	0.00592	0.01948		0.9968	0.05582
h	0.02385	0.0149	0.00265	0.01576		0.9973	0.05360
i	0.02407	0.0181	0.00436	0.01537		0.9995	0.02347
j	0.03587	0.0164	0.00489	0.00875		0.9992	0.02801
k	0.02917	0.0187	0.00834	0.01222		0.9995	0.02176
1	0.06190	0.0119	0.01160	0.00502		0.9985	0.03920
m	0.01708	0.0266	0.00474	0.02990		0.9987	0.03594
n	0.01191	0.0525	0.00182	0.02136		0.9982	0.04345
11							
Mean	0.03231	0.0295	0.00585	0.01485		0.9986	0.03664

against ex vivo pre-creep and creep data not used for curve-fitting, were not evaluated. Ideally, our model should be capable of predicting the in vivo pre-creep and creep of vaginal tissue at higher stresses while being validated using data collected in vivo at much lower stresses, since conducting creep testing at high stresses on live animals would be unethical. We acknowledge that significant adjustments to our constitutive model will be necessary to accurately represent the in vivo mechanical properties of vaginal tissue. We acknowledge that significant adjustments to our constitutive model will be necessary to accurately represent and predict the in vivo mechanical properties of vaginal tissue. For example, the active mechanical properties, particularly influenced by smooth muscle contraction, were ignored in our model formulation, but these properties have profound implications for the overall constitutive behavior of vaginal tissue. Huntington et al. [58] demonstrated that smooth muscle contraction has the ability to induce large strains in rat vaginal tissue. Similarly, a recent study by Clark-Patterson et al. [24] found that spontaneous contractions occur during creep testing of murine vaginal tissue, and that the creep behavior depends on smooth muscle tone. Despite these findings, the effects of smooth muscle tone on the viscoelastic behavior of vaginal tissue remain experimentally under-characterized. Notably, there have been no attempts to model the impact of active smooth muscle contraction on the constitutive behavior of vaginal tissue, signaling a critical research gap that warrants attention moving forward.

Several studies have suggested that the impact of pregnancy on the murine vagina goes beyond the visible changes, influencing both its microstructure and mechanical properties [12,59,60]. Since the viscoelasticity of pregnant tissue remains largely unexplored, the necessary modifications that need to be made to our constitutive equation for modeling the effects of pregnancy on the creep behavior of vaginal tissue are uncertain. Together with novel experimental techniques, advanced constitutive models that comprehensively describe

the pregnancy-induced remodeling of vaginal tissue must be developed to create new computational tools for predicting the safest mode of delivery and improving maternal care. Indeed, current computational models of rat vaginal tissue deformations only reproduce the elastic behavior of the organ [61,62], lacking any consideration of time-dependent deformations that are crucial with pregnancy.

6. Conclusions

This study presents a general single integral constitutive model for describing the creep behavior of vaginal tissue by considering the characteristic anisotropy and finite deformations of this tissue. Previously published experimental data obtained by performing consecutive freeextension inflation tests at three increasing luminal pressures were used to evaluate the constitutive model. Toward this goal, the tensorial creep function was assumed to be nonlinear and separable into the product of a time-dependent function and a stress-dependent function. Moreover, the vagina was assumed to be incompressible and subjected to normal stresses along two anatomical directions, the LD and CD. The results of the model predictions were very close to the experimental strain versus time data, demonstrating that the model can accurately illustrate the pre-creep and creep behavior of vaginal tissue in both the LD and CD. With further refinements and validation, this constitutive framework has the potential to provide insights on the time-dependent deformations of vaginal tissue. Accurate predictions of vaginal tissue deformations can inform clinical decisions related to vaginal delivery and Caesarean section procedures, fostering advancements that directly benefit the well-being of women during the critical stages of childbirth.

CRediT authorship contribution statement

Justin Dubik: Writing – review & editing, Writing – original draft, Visualization, Validation, Methodology, Investigation, Formal analysis,

Data curation, Conceptualization. Alfonsina Tartaglione: Writing – review & editing, Writing – original draft, Methodology, Investigation, Formal analysis, Conceptualization. Alan Wineman: Writing – review & editing, Writing – original draft, Methodology, Investigation, Formal analysis. David Dillard: Writing – review & editing, Writing – original draft, Supervision, Methodology, Investigation, Funding acquisition, Conceptualization. Raffaella De Vita: Writing – review & editing, Writing – original draft, Visualization, Validation, Supervision, Software, Resources, Project administration, Methodology, Investigation, Funding acquisition, Formal analysis, Data curation, Conceptualization.

Declaration of competing interest

The authors declare that they have no known competing financial interests or personal relationships that could have appeared to influence the work reported in this paper.

Data availability

Data will be made available on request.

Acknowledgments

This work was supported by the National Science Foundation, United States (Grant No. 2053851 and Grant No. 2135683), grant for joint visit (2022-2023-Call for Visiting Professors/Researchers) to Raffaella De Vita at the Università degli Studi della Campania "Luigi Vanvitelli." Alfonsina Tartaglione's research was performed under the auspices of GNFM-INdAM.

References

- M.J.K. Osterman, B.E. Hamilton, J.A. Martin, A.K. Driscoll, C.P. Valenzuela, Births: Final data for 2021, Natl. Vital Stat. Rep. 72 (1) (2023) 1–53.
- [2] J.M. Wu, C.P. Vaughan, P.S. Goode, D.T. Redden, K.L. Burgio, H.E. Richter, A.D. Markland, Prevalence and trends of symptomatic pelvic floor disorders in US women. Obstetr. Gynecol. 123 (1) (2014) 141.
- [3] J.R. Wax, A. Cartin, M.G. Pinette, J. Blackstone, Patient choice Cesarean: An evidence-based review, Obstetr. Gynecol. Surv. 59 (8) (2004) 601–616.
- [4] S.F. Meikle, C.A. Steiner, J. Zhang, W.L. Lawrence, A national estimate of the elective primary Cesarean delivery rate, Obstetr. Gynecol. 105 (4) (2005) 751–756.
- [5] M.J.K. Osterman, Changes in primary and repeat cesarean delivery: United States 2016–2021, in: National Vital Statistics Rapid Release, (no. 21) 2022.
- [6] L. Gibbons, J.M. Belizán, J.A. Lauer, A.P. Betrán, M. Merialdi, F. Althabe, et al., The global numbers and costs of additionally needed and unnecessary Caesarean sections performed per year: Overuse as a barrier to universal coverage, World Health Rep. 30 (1) (2010) 1–31.
- [7] O.E. Keag, J.E. Norman, S.J. Stock, Long-term risks and benefits associated with cesarean delivery for mother, baby, and subsequent pregnancies: Systematic review and meta-analysis, PLoS Med. 15 (1) (2018) e1002494.
- [8] I. Nygaard, Urinary incontinence: Is Cesarean delivery protective? Sem. Perinatol. 30 (5) (2006) 267–271.
- [9] K.H. Rothenberg, National institutes of health state-of-the-science conference statement: Cesarean delivery on maternal request, 107 Obstetr. Gynecol. 1386 (2006).
- [10] M.J. Grimm, Forces involved with labor and delivery—A biomechanical perspective, Ann. Biomed. Eng. 49 (8) (2021) 1819–1835.
- [11] World Health Organization, WHO Recommendations on Intrapartum Care for a Positive Childbirth Experience, World Health Organization, 2018.
- [12] A. Baah-Dwomoh, J. McGuire, T. Tan, R. De Vita, Mechanical properties of female reproductive organs and supporting connective tissues: A review of the current state of knowledge, Appl. Mech. Rev. 68 (6) (2016).
- [13] D. Ulrich, S.L. Edwards, K. Su, J.F. White, J.A.M. Ramshaw, G. Jenkin, J. Deprest, A. Rosamilia, J.A. Werkmeister, C.E. Gargett, Influence of reproductive status on tissue composition and biomechanical properties of Ovine Vagina, PLoS One 9 (4) (2014) e93172.
- [14] A.J. Huntington, B. Udayasuryan, P. Du, S.S. Verbridge, S.D. Abramowitch, R. De Vita, Smooth muscle organization and nerves in the rat vagina: A first look using tissue clearing and immunolabeling, Ann. Biomed. Eng. 50 (4) (2022) 440–451.

- [15] D. Ulrich, S.L. Edwards, V. Letouzey, K. Su, J.F. White, A. Rosamilia, C.E. Gargett, J.A. Werkmeister, Regional variation in tissue composition and biomechanical properties of postmenopausal ovine and human Vagina, PLoS One 9 (8) (2014) e104972.
- [16] C. Rubod, M. Boukerrou, M. Brieu, P. Dubois, M. Cosson, Biomechanical properties of vaginal tissue. Part 1: New experimental protocol, J. Urol. 178 (1) (2007) 320–325.
- [17] C. Rubod, M. Boukerrou, M. Brieu, C. Jean-Charles, P. Dubois, M. Cosson, Biomechanical properties of vaginal tissue: Preliminary results, Int. Urogynecol. J. 19 (6) (2008) 811–816.
- [18] E. Peña, P. Martins, T. Mascarenhas, R.M.N. Jorge, A. Ferreira, M. Doblaré, B. Calvo, Mechanical characterization of the softening behavior of human vaginal tissue, J. Mech. Behav. Biomed. Mater. 4 (3) (2011) 275–283.
- [19] C. Rubod, M. Brieu, M. Cosson, G. Rivaux, J.C. Clay, L. de Landsheere, B. Gabriel, Biomechanical properties of human pelvic organs, Urology 79 (4) (2012) 968–e17.
- [20] P. Chantereau, M. Brieu, M. Kammal, J. Farthmann, B. Gabriel, M. Cosson, Mechanical properties of pelvic soft tissue of young women and impact of aging, Int. Urogynecol. J. 25 (11) (2014) 1547–1553.
- [21] E. Peña, B. Calvo, M.A. Martínez, P. Martins, T. Mascarenhas, R.M.N. Jorge, A. Ferreira, M. Doblaré, Experimental study and constitutive modeling of the viscoelastic mechanical properties of the human prolapsed vaginal tissue, Biomech. Model. Mechanobiol. 9 (1) (2010) 35–44.
- [22] E. Pack, J. Dubik, W. Snyder, A. Simon, S. Clark, R. De Vita, Biaxial stress relaxation of vaginal tissue in pubertal gilts, J. Biomech. Eng. 142 (3) (2020) 031002.
- [23] G.L. Clark-Patterson, J.A. McGuire, L. Desrosiers, L.R. Knoepp, R. De Vita, K.S. Miller, Investigation of murine vaginal creep response to altered mechanical loads, J. Biomech. Eng. 143 (12) (2021).
- [24] G.L. Clark-Patterson, L.M. Buchanan, B.O. Ogola, M. Florian-Rodriguez, S.H. Lindsey, R. De Vita, K.S. Miller, Smooth muscle contribution to vaginal viscoelastic response, J. Mech. Behav. Biomed. Mater. 140 (2023) 105702.
- [25] J. Dubik, A. Tartaglione, K.S. Miller, D.A. Dillard, R. De Vita, History-dependent deformations of rat vaginas under inflation, Integr. Comp. Biol. 62 (2022) 625–640.
- [26] C. Jean-Charles, C. Rubod, M. Brieu, M. Boukerrou, J. Fasel, M. Cosson, Biomechanical properties of prolapsed or non-prolapsed vaginal tissue: Impact on genital prolapse surgery, Int. Urogynecol. J. 21 (2010) 1535–1538.
- [27] B. Gabriel, C. Rubod, M. Brieu, B. Dedet, L. De Landsheere, V. Delmas, M. Cosson, Vagina, abdominal skin, and aponeurosis: Do they have similar biomechanical properties? Int. Urogynecol. J. 22 (2011) 23–27.
- [28] L. de Landsheere, M. Brieu, S. Blacher, C. Munaut, B. Nusgens, C. Rubod, A. Noel, J. Foidart, M. Nisolle, Cosson. M., Elastin density: Link between histological and biomechanical properties of Vaginal tissue in women with pelvic organ prolapse? Int. Urogynecol. J. 27 (2016) 629–635.
- [29] P. Martins, E. Peña, B. Calvo, M. Doblaré, T. Mascarenhas, R. Natal Jorge, A. Ferreira, Prediction of nonlinear elastic behaviour of vaginal tissue: Experimental results and model formulation, Comput. Methods Biomech. Biomed. Eng. 13 (3) (2010) 327–337.
- [30] A.R. Akintunde, K.M. Robison, D.J. Capone, L. Desrosiers, L.R. Knoepp, K.S. Miller, Effects of elastase digestion on the murine vaginal wall biaxial mechanical response, J. Biomech. Eng. 141 (2) (2019) 021011.
- [31] B. Calvo, E. Pena, P. Martins, T. Mascarenhas, M. Doblare, R.M. Natal Jorge, A. Ferreira, On modelling damage process in vaginal tissue, J. Biomech. 42 (5) (2009) 642–651.
- [32] A.V. Kobelev, R.M. Kobeleva, Y.L. Protsenko, I.V. Berman, 2D rheological models for stress relaxation and creep in living soft tissues, Acta Bioeng. Biomech. 7 (1) (2005) 23.
- [33] S. Arıtan, S.O. Oyadiji, R.M. Bartlett, A mechanical model representation of the in vivo creep behaviour of muscular bulk tissue, J. Biomech. 41 (12) (2008) 2760–2765.
- [34] M.M. Reda Taha, S. Neidigk, A. Noureldin, Variable stiffness rheological model for interrelating creep and stress relaxation in ligaments, Int. J. Exper. Comput. Biomech. 1 (1) (2009) 96–113.
- [35] C. Truesdell, W. Noll, The Non-Linear Field Theories of Mechanics, Springer,
- [36] M.F. Beatty, Z. Zhou, Universal motions for a class of viscoelastic materials of differential type, Contin. Mech. Thermodyn. 3 (1991) 169–191.
- [37] M.F. Beatty, Z. Ziliang, Finite amplitude and free vibrations of a body supported by incompressible, nonlinear viscoelastic shear mountings, Int. J. Solids Struct. 27 (3) (1991) 355–370.
- [38] Z. Zhou, Creep and stress relaxation of an incompressible viscoelastic material of the rate type, Int. J. Solids Struct. 28 (5) (1991) 617-630.
- [39] C. Chazal, R. Moutou Pitti, Incremental constitutive formulation for time dependent materials: Creep integral approach, Mech. Time-Dependent Mater. 15 (2011) 239–253.
- [40] R.S. Lakes, R. Vanderby, Interrelation of creep and relaxation: A modeling approach for ligaments, J. Biomech. Eng. 121 (6) (1999) 612–615.
- 41] A.L. Oza, R. Vanderby, R.S. Lakes, Interrelation of creep and relaxation for nonlinearly viscoelastic materials: Application to ligament and metal, Rheol. Acta 42 (2003) 557–568.

- [42] A.L. Oza, R. Vanderby, R.S. Lakes, Creep and relaxation in ligament: Theory, methods and experiment, in: Mechanics of Biological Tissue, Springer, 2006, pp. 379–397.
- [43] A. Wineman, Nonlinear viscoelastic solids A review, Math. Mech. Solids 14 (3) (2009) 300–366.
- [44] A. Pipkin, T.G. Rogers, A non-linear integral representation for viscoelastic behaviour, J. Mech. Phys. Solids 16 (1) (1968) 59–72.
- [45] C.S. Drapaca, S. Sivaloganathan, G. Tenti, Nonlinear constitutive laws in viscoelasticity, Math. Mech. Solids 12 (2007) 475–501.
- [46] A. Muliana, K.R. Rajagopal, D. Tscharnuter, G. Pinter, A nonlinear viscoelastic constitutive model for polymeric solids based on multiple natural configuration theory, Int. J. Solids Struct. 100 (2016) 95–110.
- [47] P.P. Provenzano, R.S. Lakes, D.T. Corr, R. Vanderby, Application of nonlinear viscoelastic models to describe ligament behavior, Biomech. Model. Mechanobiol. 1 (1) (2002) 45.
- [48] R.W. Ogden, Nonlinear elasticity, anisotropy, material stability and residual stresses in soft tissue, in: Biomechanics of Soft Tissue in Cardiovascular Systems, Springer, 2003, pp. 65–108.
- [49] J. Merodio, R.W. Ogden, The influence of the invariant I₈ on the stress-deformation and ellipticity characteristics of doubly fiber-reinforced non-linearly elastic solids, Int. J. Non-Linear Mech. 41 (4) (2006) 556–563.
- [50] Y.C. Fung, Stress-strain-history relations of soft tissues in simple elongation, Biomech. Found. Object. (1972) 181–208.
- [51] Y.C. Fung, Elasticity of soft tissues in simple elongation, Am. J. Physiol. 213 (6) (1967) 1532–1544.
- [52] G.A. Holzapfel, T.C. Gasser, R.W. Ogden, A new constitutive framework for arterial wall mechanics and a comparative study of material models, J. Elast. Phys. Sci. Solids 61 (2000) 1–48.

- [53] J.A. McGuire, J.L. Monclova, A.C. Salazar Coariti, C.A. Stine, K.C. Toussaint Jr., J.M. Munson, D.A. Dillard, R. De Vita, Tear propagation in vaginal tissue under inflation, Acta Biomater. 127 (2021) 193–204.
- [54] J.A. McGuire, S.D. Abramowitch, S. Maiti, R. De Vita, Swine vagina under planar biaxial loads: An investigation of large deformations and tears, J. Biomech. Eng. 141 (4) (2019) 041003.
- [55] J.A. McGuire, C. Crandall, S. Abramowitch, R. De Vita, Inflation and rupture of vaginal tissue, Interface Focus 9 (4) (2019) 20190029.
- [56] K. Donaldson, J. Thomas, Y. Zhu, S. Clark-Deener, M. Alperin, R. De Vita, In-plane and out-of-plane deformations of gilt utero-sacral ligaments, J. Mech. Behav. Biomed. Mater. 131 (2022) 105249.
- [57] L.R.G. Treloar, Dilation of rubber on extension, Polymer 19 (12) (1978) 1414–1420.
- [58] A. Huntington, S.D. Abramowitch, P.A. Moalli, R. De Vita, Strains induced in the vagina by smooth muscle contractions, Acta Biomater. 129 (2021) 178–187.
- [59] K.T. Downing, M. Billah, E. Raparia, A. Shah, M.C. Silverstein, A. Ahmad, G.S. Boutis, The role of mode of delivery on elastic fiber architecture and vaginal vault elasticity: A rodent model study, J. Mech. Behav. Biomed. Mater. 29 (2014) 190–198
- [60] A.C. Suarez, C. Gimenez, S.R. Russell, M. Wang, J. Munson, K.M. Myers, K.S. Miller, S.D. Abramowitch, R. De Vita, Pregnancy-induced remodeling of the murine reproductive tract: A longitudinal in Vivo magnetic resonance imaging study, Sci. Rep. 14 (1) (2024) 586.
- [61] W. Snyder, J.A. McGuire, C. Mou, D.A. Dillard, T. Iliescu, R. De Vita, Data-driven variational multiscale reduced order modeling of vaginal tissue inflation, Int. J. Numer. Methods Biomed. Eng. 39 (1) (2023) e3660.
- [62] W. Snyder, A.S. Anaya, J. Krometis, T. Iliescu, R. De Vita, A numerical comparison of simplified Galerkin and machine learning reduced order models for Vaginal deformations, Comput. Math. Appl. 152 (2023) 168–180.